A Parametric Study for the Effect of Dip on Stone Mine Pillar Stability Using a Simplified Model Geometry

Gamal Rashed, NIOSH, Pittsburgh, PA
Brent Slaker, NIOSH, Pittsburgh, PA
Morgan M. Sears, NIOSH, Pittsburgh, PA
Michael M. Murphy, NIOSH, Pittsburgh, PA

Abstract

In this study, a parametric study was conducted using FLAC3D numerical models to examine the impact of oblique loading, generated from seam dip, on the strength and the failure propagation pattern of a stone pillar using two simplified geometry types. In type-1 the side walls of the pillars were assumed to be perpendicular to the roof and the floor, while in type-2 the side walls of pillars were assumed to be vertical. The complex pillar geometry in dipping mines was frequently modeled using these two geometries.

To capture a complete picture of the effect of seam dip on pillar stability, the modeled width-to-height (w/h) ratio of the pillars, in-situ stress field, and pillars roof/floor interfaces were systematically varied to account for the potential distribution of values for these parameters across the underground stone mines in United States.

Results from the numerical modeling indicate that dipping pillars have reduced strength compared to horizontal pillars. Also, an asymmetric failure propagation pattern could be obtained depending on an interaction between the w/h ratio, seam dip, in-situ stresses, and pillar geometry.

Introduction

There are about 110 operating underground stone mines in the United States that utilize the room-and-pillar mining layout with the drill-and-blast production method for the development of reserves. The main function of pillars in room-and-pillar mines is to provide both local and global stability. Local stability includes ensuring stable ribs (pillar walls) and stable roof conditions, allowing safe access to working areas. Global stability includes supporting the weight of the overburden up to the ground surface. Inadequate global stability can result in the collapse of multiple pillars over large sections of a mine, which is a catastrophic hazard (Zipf, 2001; Esterhuizen et al. 2011).

The stability of stone pillars can be influenced greatly by the overburden stresses and the occurrence of geological discontinuities (Iannacchione, 1999). Also, weak-bands in stone pillars can significantly reduce their strength, as these bands induce tension in the stronger rock slabs (Esterhuizen and Ellenberger, 2007). Discontinuity and weak-bands driven instabilities are not considered in this study.

Only stone pillar instability due to over-loading is investigated because the influence of both discontinuity features and weak-bands are highly variable and site specific. Moreover, the main purpose of this work is to more generally study the response of dip pillars to loading so that it can be applied to situations where the impact of discontinuities or weak-bands are well understood or insignificant.

Currently, there are three main methods for underground stone pillar design: empirical, analytical, and numerical methods. Empirical methods are those that rely on the back analysis of observed pillar failures. Much work has been done using this approach on the stability of coal pillars (Salamon and Munro, 1967). In 2008 NIOSH released guidelines for stone pillar design, and in 2011 NIOSH's S-pillar software program was released for analyzing pillar layouts and the effects of modifications to those layouts (Murphy et al., 2020).

The big disadvantages in empirical-based design approaches is that: (a) it is site specific, i.e., its application is restricted to the geological environment for which it was developed (Gale,1998), and (b) it relies on pillar failures to occur, i.e., a large database of pillar specific information that represents past successes and failures must exist to help obtain a reliable pillar design.

Analytical or numerical methods rely on a stress and deformation analysis of pillars and openings. The analytical methods are applicable only for simple uniform geometry and loading conditions. However, for complex mine geometries and/or loading conditions, such as inclined-seam conditions, or weak contact between the pillar/roof or pillar/floor, numerical methods provide an alternative that can be used to examine the stability of stone pillars in such conditions.

As stone mining operations continue to develop deeper and in more inclined-seams, more complex geometries for pillars and mining scenarios are generated (Newman et al., 2019). The pillar loading in such seams is subjected to

"oblique loading conditions", which is a combination of compressive and shear stresses. Oblique loading conditions can be caused by seam dip or by natural phenomena, such as faults and dykes (Martin and Maybee, 2000).

According to Suorineni et al. (2011), orebodies under both compressive and shear stresses behave very differently from those subjected to pure compression. Seam dipping was recognized by Hedley (1992) as one of the main factors that causes rockbursts. Suorineni et al. (2011) noted that pillars under oblique loading conditions are at an elevated risk of failure, as reported in cases studies by Kvapil et al. (1989); Whyatt and Varley (2008) support Suorineni's observation.

The actual underground mine geometry of dipping seam frequently developed as shown in Figure 1-a. A review of the literature revealed that some researchers/engineers (Pariseau, 1982; Martin and Maybee, 2000; Suorineni et al., 2011; Lorig and Cabrera, 2013; Suorineni et al., 2014; Jessu and Spearing, 2018) try to simplify that actual mine geometry by using either type-1 geometry shown in Figure 1-b, where the pillar ribs are perpendicular to the roof and the floor, or type-2 geometry shown in Figure 1-c, where the pillar ribs are vertical.

These two geometries are frequently used to simplify the creation of pillars in dipping mines, but they may introduce unrealistic rock failure responses. This study aims at investigating the differences in strength and the pattern of failure propagation predicted by these two simplified geometries. Ultimately, these results will be compared to models using the actual geometry as part of the following study.

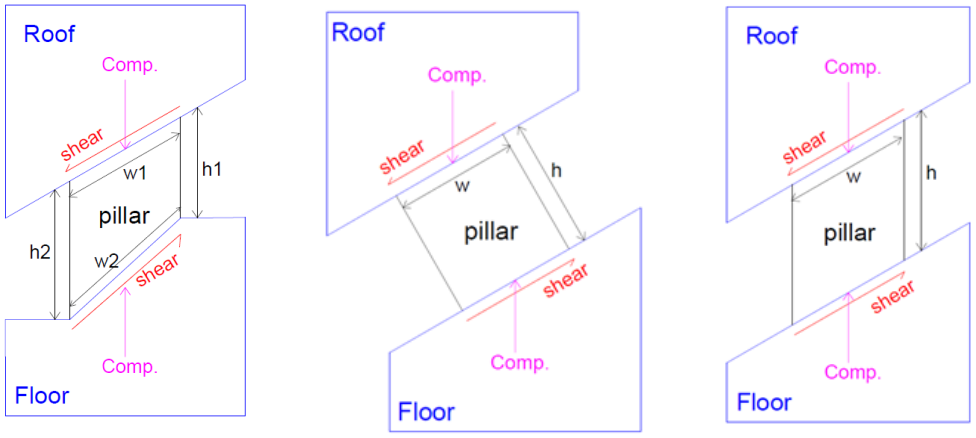

a. Actual geometry **b. Type-1 geometry** **c. Type-2 geometry**

Figure 1: Actual versus simplified pillar geometries.

The aims of this paper are to: (1) compare the pattern of failure propagation for flat-lying and dipping pillars, (2) compare the pattern of failure propagation for type-1 and type-2 geometries, (3) assess the effect of seam dip on the average strength of stone pillars of various w/h ratios and in-situ stress fields, and (4) increase awareness of the potential for pillar failure due to seam dipping.

Numerical Model Setup

An understanding of the mechanism of stone pillars fracture under oblique loading conditions is of vital interest to avoid the hazard resulting from static or dynamic pillar failures. Numerical modeling can be used to understand the effect of the two simplified geometries on the strength and failure propagation pattern of a stone pillar.

The numerical models were created using FLAC3D version 6.0 software (Itasca, 2018). The FLAC3D models can be a reliable tool if they are effectively calibrated and validated.

FLAC3D Model Calibration

In this study, a single pillar of various width-to-height (w/h) ratios in a flat-lying seam was calibrated based on empirical pillar strength equations. Abundant knowledge exists in the literature on the behavior of pillars in a flat-lying seam, which is why the FLAC3D model was calibrated to such conditions. The height of the modeled pillar was kept constant at 8.0 m (26.4 ft) to avoid changing the pillar/roof and pillar/floor constraints with changing the w/h ratio.

Therefore, to change the w/h ratio of a pillar, the width of the pillar was adjusted rather than the height. The bottom of the model is fixed, while the side boundaries are roller supported to allow only vertical movement on the sides. The model results from one pillar or array of pillars are the same if the modeled pillar(s) are in a flat-lying deposit and roller constraints are assumed at the outer vertical boundaries. The element size for the modeled stone pillar

is 0.5 m (1.64 ft). The intact rock properties for the limestone used in this paper are shown in Table 1 (Jackson et al., 1995).

Table 1: Summary for laboratory test results for the limestone used in this study.

Parameter	Value
Unconfined compressive strength (UCS), MPa	60.0
Poisson's ratio (ν)	0.25
Tensile strength (σ_t), MPa	4.76
Young's Modulus (E_i), MPa	40,800
Hoek-Brown m_i Parameter	4.9

The generalized Hoek-Brown Failure criterion was selected to model the peak strength of limestone pillars. The justification for choosing the Hoek-Brown failure criterion lies in the adequacy of its predictions of observed rock fracture behavior (Hoek et al., 2006).

The Hoek-Brown failure criterion in principal stress format is shown in Equation 1 (Hoek and Brown, 2018). There is no fundamental relationship between the empirical constants shown in Equation 1 and the physical characteristics of the rock (Hoek et al., 2006).

$$\sigma_1 = \sigma_3 + \sigma_{ci}\left[m_b\frac{\sigma_3}{\sigma_{ci}} + s\right]^a \dots\dots (1)$$

where m_b is a reduced value of the material constant m_i given by Equation 2:

$$m_b = m_i + exp\left[\frac{GSI - 100}{28 - 14D}\right] \dots\dots (2)$$

The pre-existing rock mass joints were implicitly modeled through selecting the appropriate Geological Strength Index (GSI). A peak GSI of 80 was chosen to represent a well interlocked and undisturbed limestone rock mass with rough, slightly weathered surfaces, i.e., a very good quality rock mass, and a residual GSI (GSI_r) of 26, which represents a softening of the material, was calculated from Equation 3 (Cai, 2007):

$$GSI_r = GSI * e^{(-0.0134*GSI)} \dots\dots\dots\dots (3)$$

The GSI_r represents a poorly interlocked, heavily broken residual rock mass. Given the peak/residual GSI and the disturbance factor (D), the rock mass constants s and a used in the model can be calculated from Equations 4 and 5. A disturbance factor of zero was assumed.

$$s = exp\left[\frac{GSI - 100}{9 - 3D}\right] \dots\dots (4)$$

$$a = 0.5 + \frac{1}{6}\left[e^{-\frac{GSI}{15}} - e^{-\frac{20}{3}}\right] \dots\dots (5)$$

The rock mass modulus for the modeled limestone pillars was estimated from Equation 6 (Hoek and Diederichs, 2006).

$$E_{rm} = E_i\left[0.02 + \frac{1 - \frac{D}{2}}{1 + \exp\left[\frac{60 + 15D - GSI}{11}\right]}\right] \dots\dots (6)$$

The roof and the floor material were modeled to be elastic and they were assumed to be limestone as well. Explicit interfaces representing the location of horizontal bedding planes, between the stone pillars and both the roof and floor, on which potential sliding or separation can occur were modeled. FLAC3D provides interfaces that are characterized by Coulomb sliding and/or tensile and shear bonding (Itasca, 2018). Interfaces have the properties of friction, cohesion, normal and shear stiffnesses, and tensile and shear strength as shown in Table 2. The assumed shear strength (c, φ) of the interface is weaker than the shear strength of the limestone. These interfaces were selected to represent thin shale partings within the limestone reserve, where rock can peel away after the blast.

Table 2: Interface properties used in the FLAC3D model to simulate bedding planes between pillars and roof/floor.

Parameter	Value
Normal stiffness (kn), MPa/m	13,000
Shear stiffness (ks), MPa/m	2,600
Friction angle (φ), degree	25.0
Friction-residual (φ'), degree	15.0
Cohesion (c), MPa	1.0
Cohesion-residual (c'), MPa	0.35
Tension (σ_t), MPa	0.20
Tension-residual (σ_t'), MPa	0.07

Figure 2 shows a comparison between the FLAC3D models of a flat-lying vertical pillars with a GSI of 75 and 80 and the well-known empirical pillar strength equations. As the GSI increases the quality of the rock mass increases. The scatter of pillar strength lines could be attributed to the fact that: (1) there is no unique definition for pillar-failure among the authors of these pillar strength equations and (2) the quality of the rock mass is not included in the empirical strength equations. In other words, the strength of a pillar of a given w/h ratio depends only on the scaled unconfined compressive strength, regardless of the quality of the rock mass and the in-situ stress conditions.

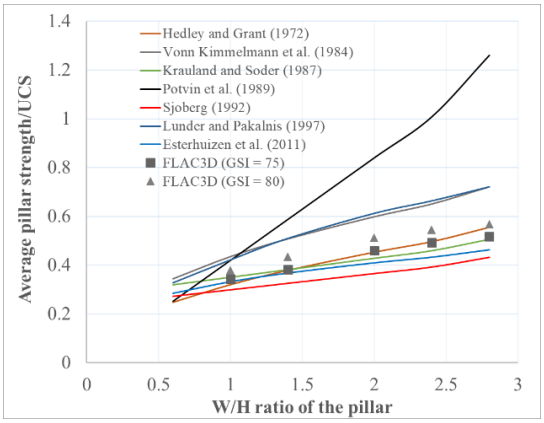

Figure 2: Comparing the FLAC3D model results with empirical pillar strength equations.

Based on the FLAC3D model results shown in Figure 2, the modeled pillar strength decreases as the rock mass quality decreases. A lower rock mass quality or unconfined compressive strength will place the pillar on a weaker pillar strength curve. Hoek and Brown's (1980) pillar strength curves for igneous crystalline rock mass shown in Figure 3 support the trend of the FLAC3D findings.

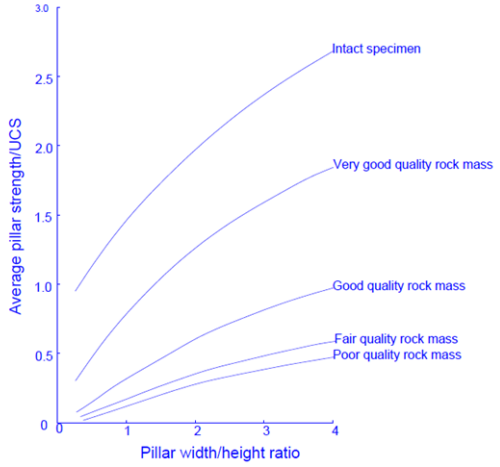

Figure 3: The effect of rock mass quality on the pillar strength of various w/h ratios (Hoek and Brown, 1980).

FLAC3D Parametric Study

Numerical modeling is a useful tool to gain additional insight into the impact of seam dip on the stability of stone pillars. Also, it can be used to examine the changing pattern of failure propagation with changing the w/h ratio of pillars, the in-situ stresses, and the interface shear strength for both type-1 and type-2 geometries.

In this study, the seam dip was changed from 0° to 40° at 10° increments. The in-situ stress field was varied to account for low and high in-situ stress fields encountered in the U.S., where the horizontal/vertical stress ratio (k-ratio) is 0.3, 1.0, and 3.0. The modeled w/h ratio of stone pillars varied from 0.5 to 2.5 to mirror the range of pillar-w/h ratios observed in most U.S. underground stone mines. It is very uncommon to find stone pillar failures with w/h ratio greater than 2.5 (Murphy et al., 2020).

The effect of interface shear strength between the pillars and roof/floor on pillar strength is well understood for pillars in flat-lying deposits (Obert and Duvall, 1967; Peng and Johnson, 1972; Rashed and Peng, 2015). However, it is not completely understood for pillars in inclined seams. Hence, to fully understand the interaction between the seam dip and the interface shear strength on stone pillar strength and the pattern of failure propagation, the FLAC3D models were solved with and without interfaces for both type-1 and type-2 geometries. Theoretically, the cases "without interfaces" mean very strong bedding planes between pillars and roof/floor, where no sliding or separation would occur.

The modeled pillars in this section represent an array of square pillars rather than one pillar because: (1) Martin and Maybee (2000) found that in dipping seam conditions, the % error in the average pillar strength is highest when one pillar is modeled and (2) Lorig and Cabrera (2013) claimed that in dipping seams, the displacement is not constrained to the vertical but will tend to occur normal to the extracted seams. Hence, according to Lorig and Cabrera, assuming roller support for the outer vertical boundaries is in correct and hence, erroneous results could be obtained if only one pillar was modeled. Consequently, in this study, a 5x5 array of pillars was generated in FLAC3D to keep the roller boundary conditions as far as possible from the study pillar, in the middle of the array.

A schematic of the 5x5 array for type-1 and type-2 simplified mine geometries used in the parametric study is shown in Figure 4. The element size of the central pillar is the same for all models to eliminate the impact of the element size on pillar strength. The strength of the study pillar (colored in red) was calculated by averaging vertical stresses for all elements composing that pillar at each time step until the pillar fails.

The Hoek-Brown material model and the element size used in the calibration stage were adopted in this section. An extraction ratio of 0.75 was assumed for all FLAC3D models where the extracted area is measured in the plan of the seam. Hence, a valid comparison for average pillar strength can be obtained at various w/h ratios and dip angles.

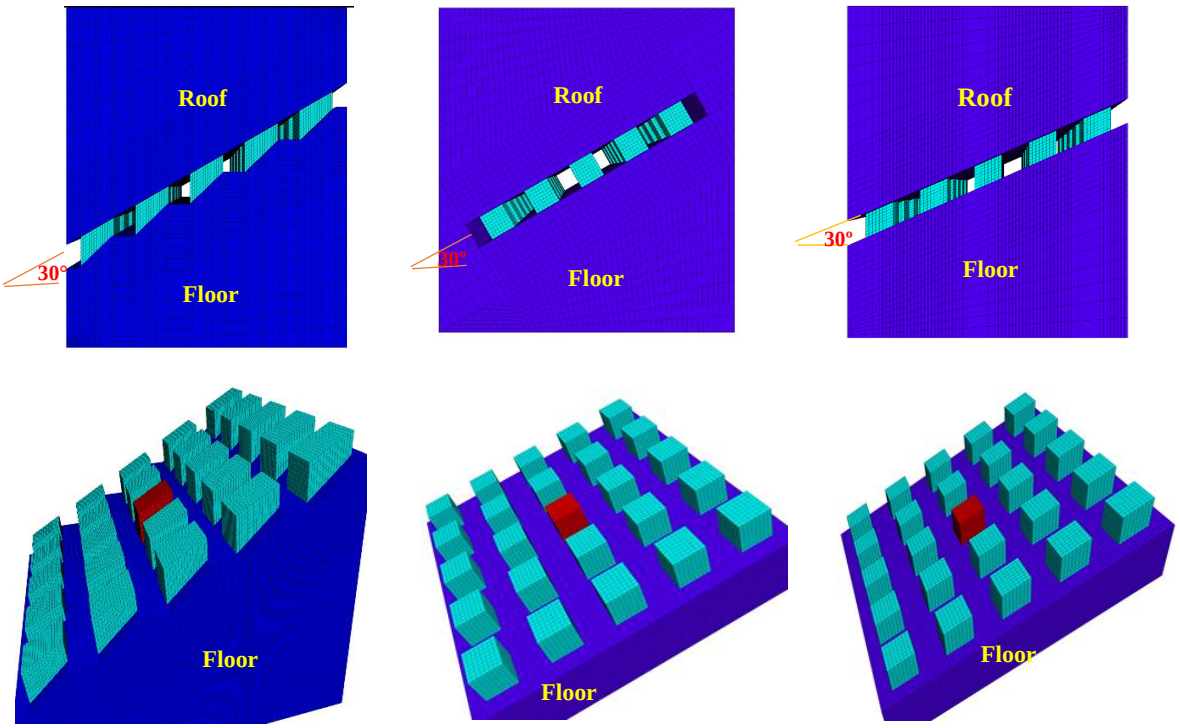

a. Actual geometry **b. Type-1 geometry** **c.Type-2 geometry**

Figure 4: Schematic for the 5x5 array of pillars, dipping at 30° for actual and simplified type geometries; the study pillar is in red.

The FLAC3D model was solved in three stages: (1) Geostatic stage, in which the pre-mining in-situ stresses are initialized; (2) Development stage, in which all headings and cross-cuts are excavated. To minimize the unrealistic damage to the region around the excavation, the "zone relax" command in FLAC3D was used to gradually excavate the material by reducing the stiffness, stresses, and densities of zones in headings/cross-cuts (Itasca, 2018); (3) Displacement loading stage, in which the top roof was moved at a very low rate (0.5E-6 m/cycle) to fail the study pillar and the residual strength is reached. In the geostatic stage, the average vertical stress for the study pillar is the same for all models irrespective of seam dip or w/h ratio. Hence, a valid comparison between models can be obtained.

Influence of Seam Dip on Pillar Strength with and without interfaces

The FLAC3D models were used to examine the effect of seam dip on stone pillar strength for type-1 and type-2 simplified geometries with and without interfaces at various w/h ratios. The shear strength of the interface used in the model is weak (see Table 2). This can be particularly important because many mines purposefully select a weak interface to define the roof line in order to reduce roof falls. Hence, the effect of seam inclination on pillar strength was examined at two extreme conditions of interface shear strength.

Figure 5 shows the variation of the average pillar strength at various seam-inclinations, when the k-ratio was 1.0 and interfaces are present. Similar behaviors were found at k-ratios of 0.3 and 3.0. However, the average pillar strength increases with increasing the k-ratio.

The nonlinear behavior shown in Figure 5 can be attributed to a number of factors: (1) using a nonlinear material model (Hoek-Brown material model); (2) using an interface between the stone pillars and the roof and the floor; (3) changing the geometry/shape of stone pillars.

Generally, pillar strength increases with increasing w/h ratio, and it decreases with increasing seam dip. The average pillar strength for the type-1 geometry is higher than the type-2 geometry, particularly at high seam dip (30º and 40º), where the right-angle of the type-1 geometry prevents the slippage on the pillar and roof/floor interfaces and hence strengthens the pillar. On the other hand, slipping along the interfaces occurs for the type-2 geometry at high seam dip.

As shown in Figure 5, for pillars of type-1 geometry, the reduction in average pillar strength is small (less than 5%) when the seam dip changes from 0º to 10°. However, the reduction is about 42% when the seam dip changes from 0° to 40°. The impact of seam dip on pillar strength does not depend on the w/h ratio for type-1 geometry.

Conversely, for type-2 geometry the impact of seam dip on the pillar strength does depend on the w/h ratio. When the w/h ratio was 0.5 or 1.0, changing the seam dip from 0º to 20º results in very little reduction in pillar strength. However, the pillar strength was reduced by 68% when the seam dip changed from 0º to 40º for a w/h ratio of 0.5. When the w/h ratio was 2.5, the average pillar strength was reduced by about 5% when the seam dip changed from 0º to 10º, while it reduced by 56% when the seam dip changed from 0º to 40º.

The average pillar strength obtained from the type-2 geometry at dip angles of 30º and 40º is significantly less than that at 10º and 20º. This is because slipping occurred on the interfaces at dip angles of 30º and 40º before the pillar's ultimate strength was reached, while it occurred at dip angles of 10º and 20º after the ultimate strength of the pillar was reached.

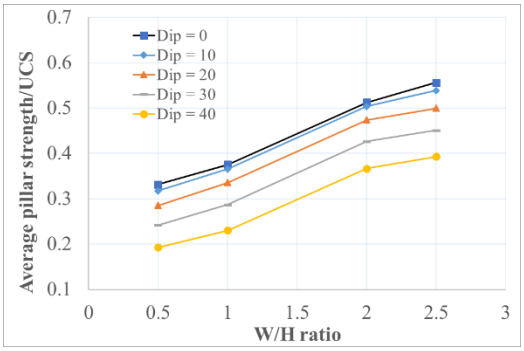

Type-1 geometry

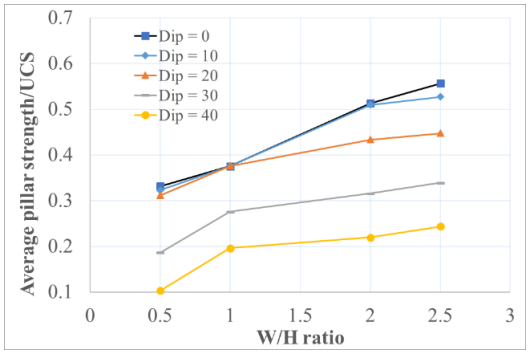

Type-2 geometry

Figure 5: Variation of average pillar strength with pillar-w/h ratios at various seam inclinations for type-1 and type-2 geometries *with interfaces*.

Figure 6 shows the variation of the average pillar strength versus w/h ratios for type-1 and type-2 geometries with no interfaces. The average pillar strength for the type-2 geometry is higher than the pillar strength for type-1 geometry, with the reason possibly being that the effective loaded area on pillars is higher for the type-2 geometry than the type-1 geometry.

For type-1 geometry, the trends for the average pillar strength with and without interfaces are similar, except that the pillar strength is higher when there are no interfaces. Hence, the impact of seam dip on pillar strength for the type-1 geometry with and without interfaces are the same. For the type-2 geometry without interfaces, when the w/h ratio is less than 2.0, the impact of seam dip on pillar strength is less important, at dip angles up to 30º when compared to the type-2 geometry with interfaces, while for a dip angle of 40º the importance of seam dip is obvious when the w/h ratio is greater than 1.0.

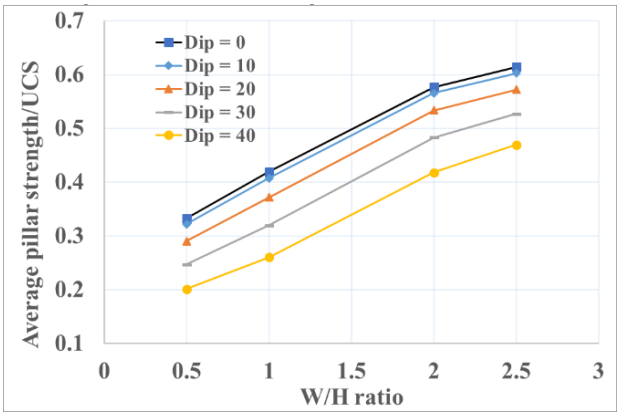

Type-1 geometry

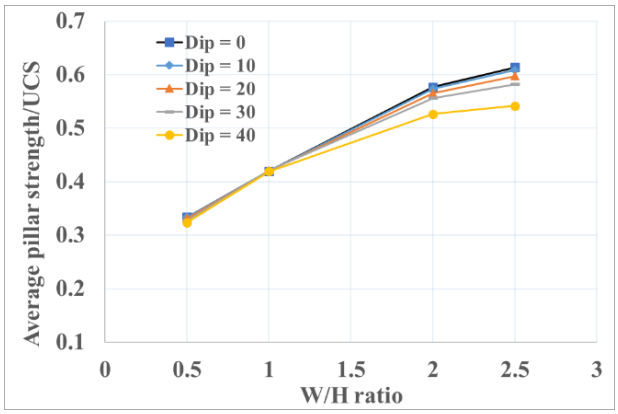

Type-2 geometry

Figure 6: Variation of average pillar strength with pillar-w/h ratios at various seam inclinations for type-1 and type-2 geometries *without interfaces*.

Effect of Seam Dip on Confining Pressure

The reduction of pillar strength with increasing seam dip is partially attributable to the reduction of the confining pressure. Figure 7 shows the variation of the minimum principal stress (σ3) versus pillar w/h ratio at various seam inclinations for the type-1 geometry with interfaces and a k-ratio of 1.0. Here, positive values for σ3 mean compression. It is apparent that the minimum principal stress decreases with increasing the pillar inclination. Hence, stone pillars become less stable as the pillar inclination increases. Similar trends were found at k-ratios of 0.3 and 3.0.

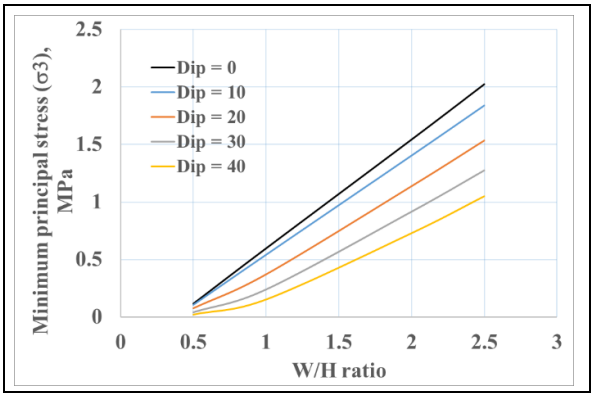

Figure 7: Variation of the minimum principal stress with w/h ratio at various seam inclinations for the type-1 geometry with interfaces and a k-ratio of 1.0.

The lateral confining stress generated from the k-ratio has the effect of strengthening the pillar. Any increase of the k-ratio will reduce or prevent slippage along the pillar/roof and pillar/floor interfaces and increase the confining pressure as shown in Figure 8.

Therefore, the strength and stability of stone pillars increases with increasing the k-ratio. A combination of low k-ratio, low pillar w/h ratio, and high seam dip may result in a very low minimum principal stress or a tensile minimum principal stress as shown in Figure 8.

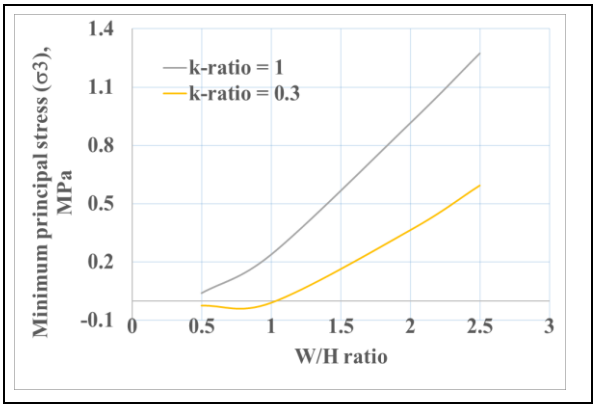

Figure 8: Variation of the minimum principal stress with w/h ratio at 30 dip for the type-1 geometry with interfaces and a k-ratio of 0.3 and 1.

Influence of Seam Dip on the Failure Propagation Pattern

The fracture propagation in stone pillars has considerable practical significance in relation to the overall excavation stability. To understand the mechanics of stress-induced instability in stone pillars and the measures required to control that instability, it is necessary to understand the patterns of fracture propagation.

For pillars in flat-lying deposits, the failure pattern starts at the pillar corners/edges and propagates uniformly towards the core of the pillar in a symmetric manner as shown in Figure 9, irrespective of the k-ratio, pillar w/h ratio, and interface shear strength between the pillar and the roof/floor.

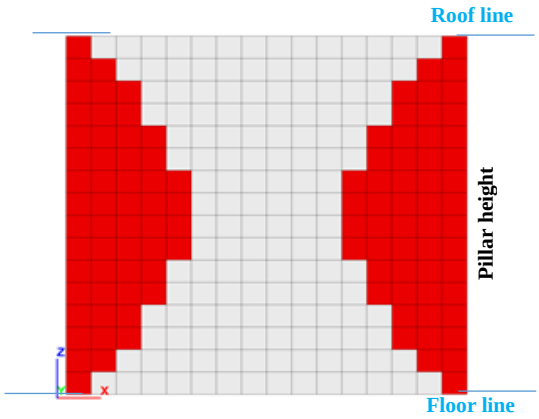

Figure 9: Symmetric failure propagation pattern for a pillar in a flat-lying seam (red elements are yielded).

On the hand, if the seam dip is non-zero, other factors start to play a role in the sequence of the failure propagation pattern. The interaction among these factors controls the sequence of fracture propagation. When mining in an inclined seam, the stress field acting on the excavations and the pillars between excavations is no longer aligned normal and parallel to the excavation boundaries as in the case of flat-lying seams (Hoek and Brown, 1980). The inclination of the stress field relative to the excavation boundaries results in a considerable shear stresses parallel to the dip of the seam, which give rise to asymmetrical shear stress distribution. The following discussion of the failure propagation pattern is limited to stone pillars of w/h ratio 0.5 and 1.0 with and without interfaces when the seam dip ranges from 10º to 40º.

Failure Propagation Pattern for Pillars of W/H Ratio = 0.5

For pillars of w/h ratio = 0.5 of the type-1 geometry, the pattern of failure propagation starts at two opposite

corners and propagates down dip along the diagonal towards the pillar core as shown in Figure 10a. The pillar diagonals are equal for type-1 geometry, which is why the failure commences at the highest point of the pillar.

Conversely, for type-2 geometry the failure pattern did not propagate along the down dip diagonal but started at the corners of the short diagonal and propagated along that diagonal toward the pillar core as shown in Figure 10b. The load path is always looking for the stiffest, shortest direction to transfer the load. For both type-1 and type-2 geometries, the direction of the major principal stress coincides with the direction of failure propagation.

The failure propagation pattern shown in Figure 10 did not change with increasing the k-ratio to 1.0 or 3.0. Suorineni et al. (2014) claimed that pillars under oblique loading conditions are at an elevated risk of catastrophic failure. The reason for such catastrophic failure could be attributed to a shear failure that passes through the pillar core as shown in Figure 10

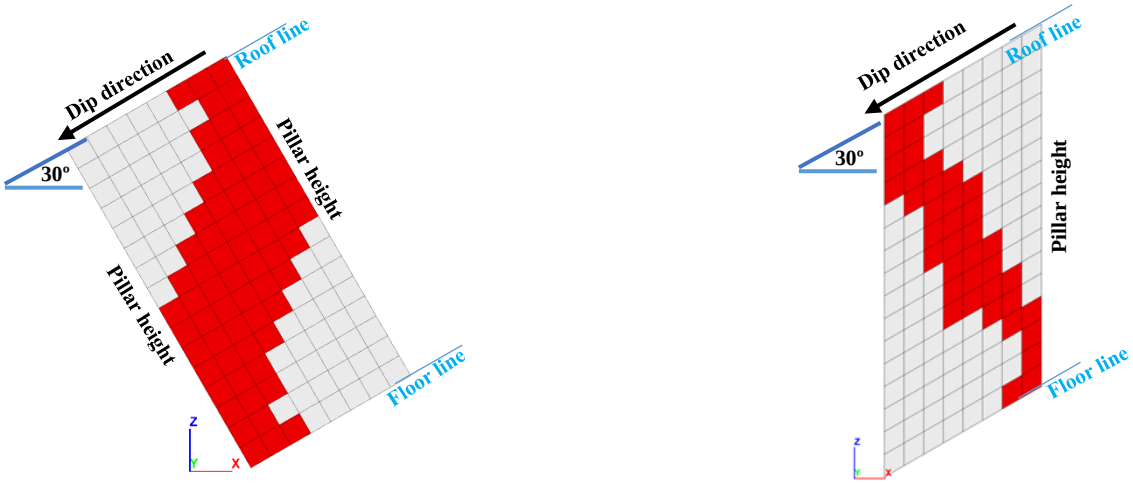

a. Type-1 geometry

b. Type-2 geometry

Figure 10: Asymmetric failure propagation for w/h ratio = 0.5, dip angle = 30°, and k-ratio = 0.3 for type-1 and type-2 geometries *with interfaces* (red elements are yielded).

Failure Propagation Pattern for Pillars of W/H Ratio = 1.0

For pillars of w/h ratio = 1.0 of the type-1 geometry, the pattern of failure propagation was asymmetric as shown in Figure 10a when the k-ratio was = 0.3 or 1.0. However, when the k-ratio was 3.0, the pattern of failure propagation started as asymmetric. However, the failure pattern became symmetric, as shown in figure 11 when the applied load was close to the pillar ultimate strength. The observed patterns did not change with increasing the interface shear strength from models "with interfaces" to "without interfaces".

For type-2 geometry, when the k-ratio is 0.3 or 1.0 and seam dip is 10° or 20°, the failure propagation pattern started at the corners of the shortest diagonal of the pillar as shown in Figure 12a, no slipping occurs along the interfaces at the 10° and 20° dip angles until the pillar ultimate strength is reached.

With increasing the applied load, more yielding occurs at the side walls of the pillar, not along the pillar core, and the failure pattern becomes more symmetric. Conversely, for the k-ratio = 3.0, the failure propagation pattern not only follows the shortest diagonal but also passes through the pillar core, as shown in Figure 12b.

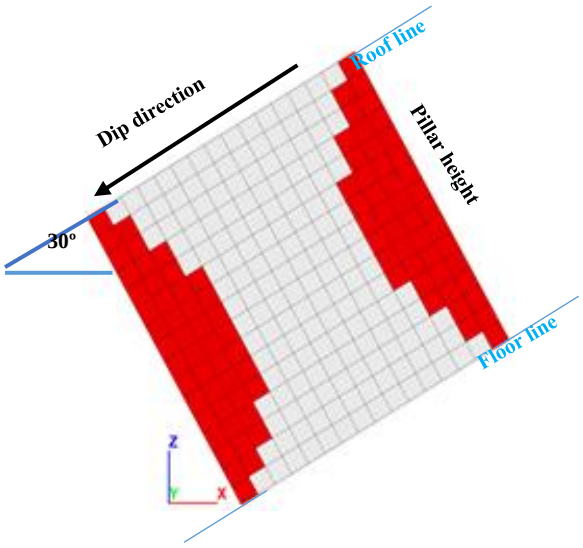

Figure 11: Symmetric failure propagation pattern for type-1 geometry *with interfaces* when w/h ratio = 1.0, dip angle = 30°, and k-ratio = 3.0 (red elements are yielded).

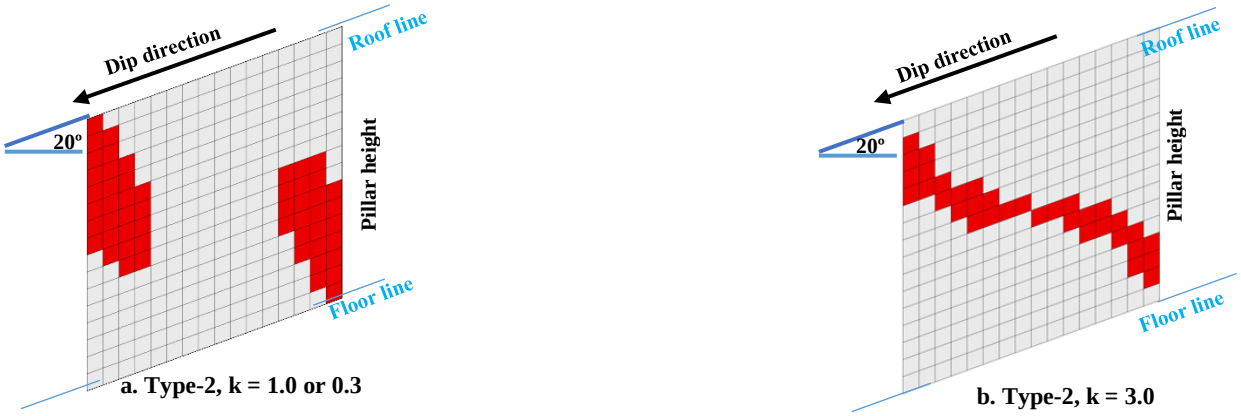

Figure 12: Asymmetric failure propagation for type-2 geometry *with interfaces* for w/h ratio = 1.0, dip angle = 20°, and a) k-ratio = 0.3 or 1.0 and b) k-ratio = 3.0 (red elements are yielded).

On the other hand, when the k-ratio is 0.3 or 1.0 and the seam dip is 30° or 40°, slipping occurs along the interfaces at the corners of the long diagonal before pillar-ultimate strength is reached. The size of the slipping zone depends on the seam dip and the k-ratio. The higher the seam dip, the larger the slipping zone and the higher the k-ratio, the smaller the slipping zone. Failure of the pillar commences at the end of the slipping zone and predominately propagates down dip along the pillar core as shown in Figure 13. Conversely, when the k-ratio is 3.0, the failure propagates along the short diagonal, because slipping along the interface is prevented at that k-ratio.

Figure 13: Asymmetric failure propagation for type-2 geometry *with interfaces* for w/h ratio = 1.0, dip angle = 30°, and k-ratio of 0.3 or 1.0 (red elements are yielded).

For type-2 geometry with no interfaces or very strong interfaces, when the k-ratio is 0.3 or 1.0, the failure stated as asymmetric at the corners of the short diagonal as shown in Figure 14a, but with increasing the applied load, it becomes symmetric as shown in Figure 14b, while the failure propagation pattern is asymmetric and passes by the pillar core when the k-ratio is 3.0 as shown in Figure 14c. Hence, for pillars of type-1 and type-2 geometries, the pattern of failure propagation might be asymmetric depending on an interaction between seam dip, pillar w/h ratio, k-ratio, and pillar/roof and pillar/floor shear strength. An asymmetric fracture propagation that passes through the pillar core not only reduced the ultimate strength of the stone pillar but may also place the stone pillar at an elevated risk of instability.

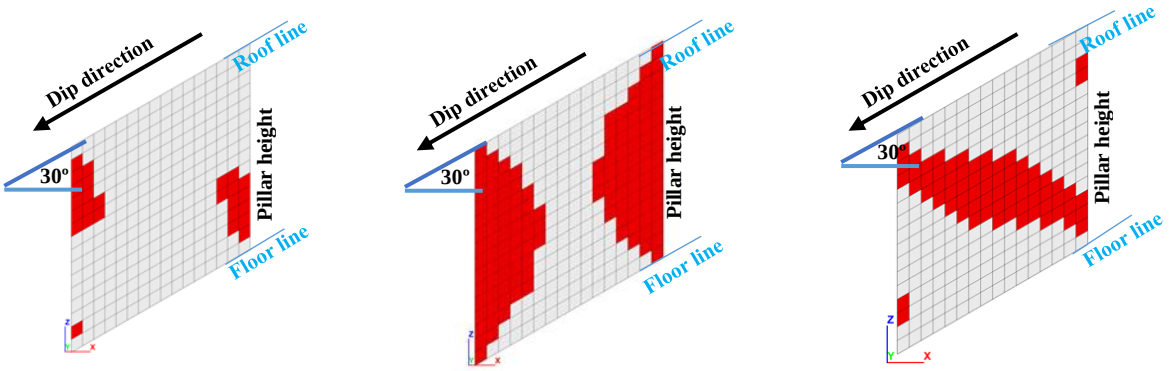

a. Asymmetric pattern, load < pillar-capacity. k-ratio = 0.3 or 1.0

b. Asymmetric pattern, load close to pillar-capacity. k-ratio = 0.3 or 1.0

c. Asymmetric pattern, k-ratio = 3.0

Figure 14: Pattern of failure propagation for type-2 geometry *without interfaces* for w/h ratio = 1.0, dip angle = 30º, and k-ratio = 0.3 or 1.0 (red elements are yielded).

Summary and Conclusions

This study was conducted using FLAC3D models to compare the strength and the failure propagation patterns for two simplified pillar geometries. These two simplified geometries, type-1 and type-2, are used in the literature to simplify the actual/complex pillar geometry in dipping mines. The side walls of the pillars are perpendicular to the roof and the floor for the type-1 geometry, while for type-2 geometry the side walls are vertical.

In this study, the seam dip ranges from 0° to 40°. The in-situ stress field was varied to account for low and high in-situ stress fields encountered in the United States, where the horizontal/vertical stress ratio (k-ratio) is 0.3, 1.0 and 3.0. The modeled width-to-height (w/h) ratio of stone pillars ranges from 0.5 to 2.5 to mirror the range of pillar-w/h ratios observed in most U.S. underground stone mines. The FLAC3D models were solved with and without interfaces between stone pillars and the roof/floor to replicate weak and strong interface shear strength.

The main conclusions of this study can be summarized in the following points:

- The strength of a stone pillar deceases as the seam dip increases, while it increases with increasing the k-ratio and the w/h ratio.
- The impact of seam dip on pillar strength depends on the dip angle, the interface shear strength, the w/h ratio, and the simplified geometry used to model the actual pillar geometry.
- There is insignificant reduction in pillar strength, (less than 5%) when the seam dip changed from 0º to 10º for both type-1 or type-2 geometries.
- The strength of a stone pillar predicted from the type-1 geometry tends to be significantly higher than that predicted from the type-2 geometry for high dip angles when interfaces exist between pillars and the roof/floor. The opposite is true when interfaces between the pillar and roof/floor are not present at all dip angles.
- For flat-lying pillars, the failure pattern starts at the pillar corners/edges and propagates uniformly towards the core of the pillar in a symmetric manner irrespective of the k-ratio, w/h ratio, and roof/floor shear strength.
- For pillars of w/h ratio = 0.5 in oblique loading conditions, the fracture pattern is always asymmetric. It propagates along the short diagonal towards the pillar core for type-2 geometry, while for type-1 geometry it propagates down dip along the opposite corners towards the pillar core.
- For pillars of w/h ratio = 1.0 in oblique loading conditions, the pattern of fracture propagation is contingent on several factors, such as the seam dip, the simplified geometry used to model the pillar, the w/h ratio, the k-ratio, and the presence or absence of interfaces between pillars and roof/floor.
- Pillars under oblique loading conditions are at an elevated risk of instability because of the asymmetric failure propagation that passes through the pillar core.

Disclaimer

The findings and conclusions in this paper are those of the authors and do not necessarily represent the official position of the National Institute for Occupational Safety and Health, Centers for Disease Control and Prevention.

References

Cai, M. (2007). “Determination of residual strength parameters of jointed rock masses using the GSI system." International Journal of Rock Mechanics & Mining Sciences, no. 44, pp. 247-265.

Esterhuizen, G.S. and Ellenberger, J.L. (2007). “Effects of weak bands on pillar stability in stone mines: Field observations and numerical model assessment”. Proceedings of the 26th International Conference on Ground Control in Mining, Morgantown, West Virginia. pp. 320-326.

Esterhuizen, G.S., Dolinar, D.R., and Ellenberger, J.L. (2011). “Pillar strength in underground stone mines in the United States”. International Journal of Rock Mechanics and Mining Sciences 48(1): pp. 42-50.

Gale, W.J. (1998). “Coal pillar design issues in longwall mining”. In Aziz, N(ed), coal operators’ conference, University of Wollongong & the Australasian Institute of Mining and Metallurgy, pp. 133-146.

Hedley, D.G.F. (1992). “Rockburst Handbook for Ontario Hardrock Mines”. CANMET Special Report SP92- 1E. Canada Communication Group, Ottawa. pp:23 1-242.

Hedley, D.G.F. and Grant, F. (1972). “Stope and pillar design for the Elliot lake uranium mines”. CIM Bulletin, vol. 65. pp. 37–44.

Hoek, E. and Brown, E.T. (1980). “Underground excavations in rock”. Published by the Institute of Mining and Metallurgy. London, England. pp.526.

Hoek, E. and Brown, E.T. (2018). “The Hoek-Brown failure criterion and GSI – 2018 edition”. Journal of Rock Mechanics and Geotechnical Engineering. doi: 10.1016/j.jrmge.2018.08.00.

Hoek, E., and Diederichs, M.S. (2006). “Empirical estimation of rock mass modulus”. International Journal of Rock Mechanics and Mining sciences. Vol. 43, Issue 2, pp. 203-2015.

Hoek, E., Kaiser, P.K., and Bawden, W.F. (2006). “Support of underground excavations in hard rock”. Published by Taylor & Francis. pp. 215.

Iannacchione,T. (1999). “Analysis of pillar design practices and techniques for U.S. limestone mines”. Trans. Inst. Min. Metall. (sect. A: Min. Industry), September–December 108: A152– A160.

Itasca Consulting Group. (2018). “Fast Lagrangian Analysis of Continua in 3Dimensions”; Itasca Consulting Group: Minneapolis, MN, USA.

Jackson, R., Gorski, B., and Gyenge, M. (1995). “Geotechnical Properties of Rock: A Data Base of Physical Properties of Canadian Rock Including Both Intact and Residual Strengths”. Published by Canada Communication Group. pp. 15-91.

Jessu, K.V. and Spearing, A.J.S. (2018). “Effect of dip on pillar strength”. the Journal of the Southern African Institute of Mining and Metallurgy, vol. 118, pp. 765-776.

Krauland, N. and Soder, P. (1987). “Determining pillar strength from pillar failure observation”. E&MJ. pp. 34-40.

Kvapil, R. L., Beaza, J. R. and Flores, G. (1989). Block caving at EI Teniente Mine, Chile, Inst. Min. Metall., 98, (6), A43–A56.

Lorig, L. J., and Cabrera, A. (2013). “Pillar Strength Estimates for Foliated and Inclined Pillars in Schistose Material,” in Continuum and Distinct Element Numerical Modeling in Geomechanics. (CD Proceedings, 3rd International FLAC/DEM Symposium, Hangzhou, China, October 2013). Paper: 01-01, H. Zhu et al., Eds. Minneapolis: Itasca International, Inc.

Lunder, P. J. and Pakalnis, R. C. (1997). “Determination of the strength of hard-rock mine pillars”. Bull. Can. Inst. Min. Metall., 90(1013). pp. 51-55.

Martin, C.D. and Maybee, W.G. (2000). “The strength of hard rock pillars”. International Journal of Rock Mechanics and Mining Sciences, vol. 37. pp. 1239–1246.

Newman, C., Newman, D., and Dupuy, R. (2019). “The development of a multiple level underground limestone mine from geology through mine planning”. Proceedings of the 38th International Conference on Ground Control in Mining. Pp. 116-121.

Obert, L. and Duvall, W. (1967). “Rock mechanics and the design of structure in rock”. John Wiley & Sons, Inc., New York. pp. 650.

Pariseau, W.G. (1982). “Shear stability of mine pillars in dipping seams”. 23rd U.S. Symposium on Rock Mechanics (USRMS). Berkeley, California.

Peng, S.S., and Johnson, A.M. (1972). “Crack growth and faulting in cylindrical specimens of Chelmsford Granite”. International Journal of Rock Mechanics and Mining Science, 9(1), pp. 37-86.

Potvin, Y., Hudyrna, M., and Miller, H.D.S. (1989). “Rib pillar design in open stope minining”. Bull. Can. Inst. Min. Metall., vol. 82, No. 927: 31-36.

Rashed, G. and Peng, S.S. (2015). “Change of the mode of failure by interface friction and width-to-height ratio of coal specimens”. Int. Journal of Rock Mechanics and Geotechnical Engineering. Vol. 7, Issue 3. pp 256-265.

Salmon, M.D.G., and Munro, A.H., (1967). “A Study of the Strength of Coal Pillars”. South Afr. Inst. Min. Metall., 68:55-67.

Sjoberg, J. (1992). “Failure modes and pillar behaviour in the Zinkgruvan mine”. Rock Mechanics, Tillerson & Wawersik (eds). Balkema, Rotterdam.

Suorineni, F.T., Mgumbwa, J.J., Kaiser, P.K., and Thibodeau, D. (2011). “Mining of orebodies under shear loading. Part 1 – case histories”. Transactions of the

Institution of Mining and Metallurgy. Section A: Mining Technology, vol. 120, no. 3. pp. 138–147.

Von Kimmelmann, M.R., Hyde, B., and Madgwick, R.J. (1984). "The use of computer applications at BCL Limited in planning pillar extraction and the design of mining layouts. Design and performance of underground excavations". ISRM/BGS, Cambridge, pp- 53-63.

Whyatt, J. and Varley, F. (2008). "Catastrophic failures of underground evaporite mines", Proc. 27th Int. Conf. on Ground control in mining, Morgantown, WV. pp. 113–122.

Zipf, R. K. (2001). "Pillar design to prevent collapse of room-and-pillar mines". In: Hustrulid WA, Bullock RC, editors. Underground mining methods: engineering fundamentals and international case studies. Denver: Soc. Min. Metall. Expl.; pp. 493–511.